Comparative study of upper critical field H_{c2} and second magnetization peak H_{sp} in hole- and electron-doped $BaFe_2As_2$ superconductor

D. L. Sun, Y. Liu, and C. T. Lin
Max-Planck-Institut für Festkörperforschung, Heisenbergstr. 1, D-70569 Stuttgart, Germany
(Received 29 July 2009; revised manuscript received 10 September 2009; published 12 October 2009)

A comparative study of the upper critical field H_{c2} and second magnetization peak H_{sp} was performed using high-quality single crystals of hole-doped $Ba_{0.68}K_{0.32}Fe_2As_2$ and electron-doped $BaFe_{1.85}Co_{0.15}As_2$ and $BaFe_{1.91}Ni_{0.09}As_2$. The H_{c2} was extracted from both resistivity and magnetization measurements using varying magnetic fields on $H\|c$ and $H\perp c$ orientations. The anisotropic ratio, $\gamma=H_{c2}^{\perp c}/H_{c2}^{\|c}$, was observed to decrease to ~2.5 for the hole-doped and ~3.0 for both electron-doped samples as the magnetic fields were increased up to 9 T. It demonstrates that the anisotropic properties only show slight change by doping aliovalent ions either in or out-of the basal plane of FeAs. For the hole-doped $Ba_{0.68}K_{0.32}Fe_2As_2$ the H_{c2} and H_{sp} shift toward the higher temperature and higher field regime in the temperature-normalized (T/T_c) vortex phase diagram, suggesting a stronger vortex pinning by the comparison with the electron-doped $BaFe_{1.85}Co_{0.15}As_2$ and $BaFe_{1.91}Ni_{0.09}As_2$. In contrast to the As-deficiency or inhomogeneous doping distribution of K, Co, and Ni, the dense pinning centers in $Ba_{0.68}K_{0.32}Fe_2As_2$ may be attributed to the disordered structural domains and suggested to be responsible for the intrinsic disorder and anisotropy of iron arsenides.

DOI: 10.1103/PhysRevB.80.144515 PACS number(s): 74.70.Dd, 74.25.Op, 74.25.Qt

I. INTRODUCTION

The investigations on the upper critical field H_{c2} for the iron-based superconductors are crucial to study their superconducting mechanism and explore potential application aspects. Basically, one can estimate the zero temperature $H_{c2}(0)$ with the classical Werthamer–Helfand–Hohenberg (WHH) expression $H_{c2}(0)=-0.69T_c(dH_{c2}/dT)_{T_c}$,[1] and then calculate the coherence length ξ with the Ginzburg–Landau relations, $H_{c2}^{\|c}=\phi_0/2\pi\xi_{ab}^2$ and $H_{c2}^{\perp c}=\phi_0/2\pi\xi_{ab}\xi_c$, in layered superconductors.[2] Since the discovery of iron-based superconductors,[3] considerable attention has been focused on the analysis of H_{c2} for $ReFeAsO_{1-x}F_x$ (Re: rare-earth elements),[4–7] $Ba_{1-x}K_xFe_2As_2$,[8–13] and $BaFe_{2-x}Co_xAs_2$ [14–16] compounds through the measurement of their resistivity, heat-capacity, and radio-frequency penetration depth. The iron-based superconductors exhibit a huge upper critical field H_{c2} beyond 100 T, deduced from high magnetic field data.[4,7] In contrast to a large anisotropic ratio observed in high-T_c cuprates, a nearly isotropic H_{c2} $(\gamma=H_{c2}^{\perp c}/H_{c2}^{\|c}\approx 1\sim 2)$ at low temperature was observed for the iron-based superconductors from the high magnetic field data, which fields applied perpendicular and parallel to the c axis of the samples.[11,13,14,16] Furthermore, a positive curvature is observed in temperature dependence of H_{c2} and qualitatively explained by the two-band model.[4,7] However, the isotropic H_{c2} obviously seems to contradict the two-band model because the anisotropy should increase with decreasing temperature in the latter.[12]

In addition to the above-mentioned methods to extract H_{c2}, one can determine H_{c2} from the temperature dependence of the magnetization under varying magnetic fields. Up to now, there has been no report on the analysis of magnetically determined $H_{c2}(T)$ for iron-based superconductors. In general, the magnetic measurements mainly reflect the bulk superconductivity of the samples. Therefore, we present a comparative analysis of H_{c2} on both hole-doped $Ba_{0.68}K_{0.32}Fe_2As_2$ and electron-doped $BaFe_{1.85}Co_{0.15}As_2$ and $BaFe_{1.91}Ni_{0.09}As_2$ single crystals in this work. The magnetically determined $H_{c2}(T)$ is extracted from the temperature dependence of the magnetization (M vs T) under varying magnetic fields for both $H\|c$ and $H\perp c$ orientations. The anisotropic ratio $\gamma=H_{c2}^{\perp c}/H_{c2}^{\|c}$ obtained by the magnetic measurements coincides with that obtained by resistivity measurements. The second magnetization peak and critical current density J_c are used for a further comparison between the hole-doped and electron-doped single crystals. Our results confirm that there is no significant change of the anisotropy ratio either by doping in or out-of the FeAs layer. Strong vortex pining is observed in $Ba_{0.68}K_{0.32}Fe_2As_2$ single-crystal characteristic of highest T_c, which sheds light on the mechanism of intrinsic vortex pinning in iron-based superconductors.

II. EXPERIMENT

The crystals were obtained by the self-flux method. The growth details were reported elsewhere.[17,18] The composition of the sample was determined by energy-dispersive x-ray spectroscopy and the results were reproducible. Resistivity measurements were performed by a physical property measurement system (PPMS) (Quantum Design) and a standard four-probe method under magnetic fields up to 9 T for both $H\|c$ and $H\perp c$ orientations. dc magnetization measurements were carried out using a superconducting quantum interference device-vibrating-sample magnetometer (SQUID-VSM) (Quantum Design) with magnetic fields up to 7 T for both $H\|c$ and $H\perp c$ orientations. For the temperature dependence of magnetization measurements, the data were collected with zero-field-cooling mode during warming process. For the measurements of magnetic hysteresis loops (MHLs), the magnetic field was swept at a speed of 200 Oe/s for the $H\|c$ orientation.

III. RESULTS AND DISCUSSION

Both single crystals of hole-doped $Ba_{0.68}K_{0.32}Fe_2As_2$ and electron-doped $BaFe_{1.85}Co_{0.15}As_2$ and $BaFe_{1.91}Ni_{0.09}As_2$ ex-

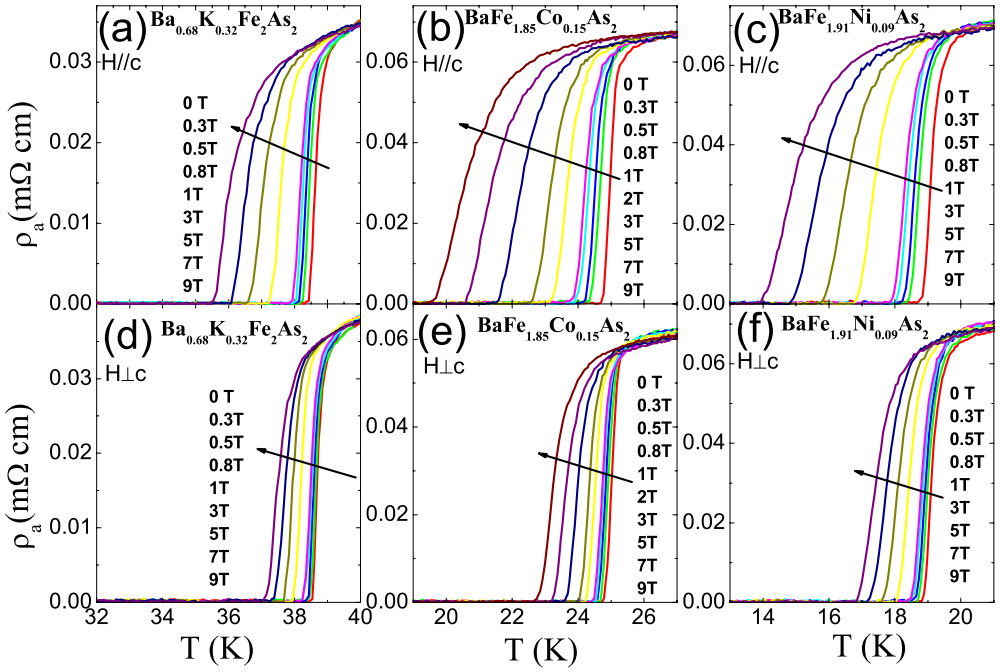

FIG. 1. (Color online) Broadening resistivity curves for both $H\|c$ and $H\perp c$ configurations. (a) and (d) for $Ba_{0.68}K_{0.32}Fe_2As_2$, (b) and (e) for $BaFe_{1.85}Co_{0.15}As_2$, and (c) and (f) for $BaFe_{1.91}Ni_{0.09}As_2$ single crystals, respectively.

hibited superconducting transition temperatures at 38.5, 24.5, and 18.5 K using magnetization measurements, respectively. These T_c values correspond to the optimally doping levels in the phase diagrams of $Ba_{1-x}K_xFe_2As_2$, $BaFe_{2-x}Co_xAs_2$, and $BaFe_{2-x}Ni_xAs_2$.[19–22] The highest T_c values are obtained for the samples doped with K and Co, when compared to those reported in the literature for the series of $Ba_{1-x}K_xFe_2As_2$ and $BaFe_{2-x}Co_xAs_2$ compounds. The T_c for Ni-doped sample is ~1.5 K lower than that reported in Ref. 22. Furthermore, extremely sharp superconducting temperature transition widths at $\Delta T_c \leq 0.4$ K for $Ba_{0.68}K_{0.32}Fe_2As_2$, $\Delta T_c \leq 0.6$ K for $BaFe_{1.85}Co_{0.15}As_2$ and $\Delta T_c \leq 1$ K for $BaFe_{1.91}Ni_{0.09}As_2$ were obtained for the single crystals, respectively. These data indicated that the high quality single crystals were reliable for further measurements.

Figures 1(a)–1(f) show the broadening resistivity curves obtained under different magnetic fields for both $H\|c$ and $H\perp c$ orientations. For $H\|c$, ρ_a displays a pronounced broadening behavior at ~3.5 K for $Ba_{0.68}K_{0.32}Fe_2As_2$, ~5.0 K for $BaFe_{1.85}Co_{0.15}As_2$ and $BaFe_{1.91}Ni_{0.09}As_2$ measured under 9 T magnetic field, as shown in Figs. 1(a)–1(c), respectively. For $H\perp c$, ρ_a shifts ~1.5 K for $Ba_{0.68}K_{0.32}Fe_2As_2$, ~2.0 K for $BaFe_{1.85}Co_{0.15}As_2$ and $BaFe_{1.91}Ni_{0.09}As_2$ single crystals toward the low temperature region, as shown in Figs. 1(d)–1(f), respectively.

Figures 2(a)–2(f) show the temperature dependence of magnetic susceptibility under different magnetic fields for both $H\|c$ and $H\perp c$ orientations. The superconducting volume fractions are nearly 100% with a 10 Oe magnetic field for all the three samples, suggesting a bulk nature of the superconductivity. The onset superconducting transition temperature rapidly decreases with increasing magnetic fields in the orientation of $H\|c$ while it shows a slow decrease in $H\perp c$. These results are consistent with the resistivity measurements. Meanwhile, the superconducting volume fractions shrink obviously with increasing magnetic fields.

The upper critical field H_{c2} was obtained by different methods and the results are shown in Figs. 3(a)–3(c), respectively. The resistive upper critical field H_{c2} was determined as the normal-state resistivity ρ_n decreases by $10\%\rho_n$ and $90\%\rho_n$, denoted with H10 and H90 in Figs. 3(a)–3(c). We also extracted the mean field $T_c(H)$, denoted as Hd, from the peak value for the plots of $d\rho/dT$ vs T. The magnetic upper critical field H_{c2} is obtained according to the onset transition temperature from the magnetic-susceptibility curves, denoted as Hm. Compared to the resistive upper critical field H_{c2}, the magnetic upper critical field H_{c2} shifts toward the lower temperature and lower field region. With decreasing temperature, magnetically determined H_{c2} decreases faster than resistive H_{c2}. The magnetic measurement mainly reflected the bulk superconductivity of the samples while higher T_c can be observed by resistivity measurement due to the net conductivity among the fluctuating domains with different T_c distributions. It should be pointed out that the H_{c2} values are different between resistivity and magnetic susceptibility data, e.g., comparison of Hm to H10. Under zero magnetic field, the difference of T_c between the two measurements data is ~1 K, which might be caused by a systematic error of temperature records in PPMS and VSM-SQUID.

In Figs. 3(a)–3(c), H10 and Hm exhibit a positive curvature while H90 and Hd show a linearlike behavior. Obviously, the plots of H10 and Hm can lead to an extremely large H_{c2} due to strong positive curvature. Here, zero-temperature upper critical field $H_{c2}(0)$ was calculated from the plot of Hd according to the WHH formula, as listed in Table I. The $H_{c2}(0)$ for $Ba_{0.68}K_{0.32}Fe_2As_2$ is about 2–4 times larger than those of electron-doped $BaFe_{1.85}Co_{0.15}As_2$ and

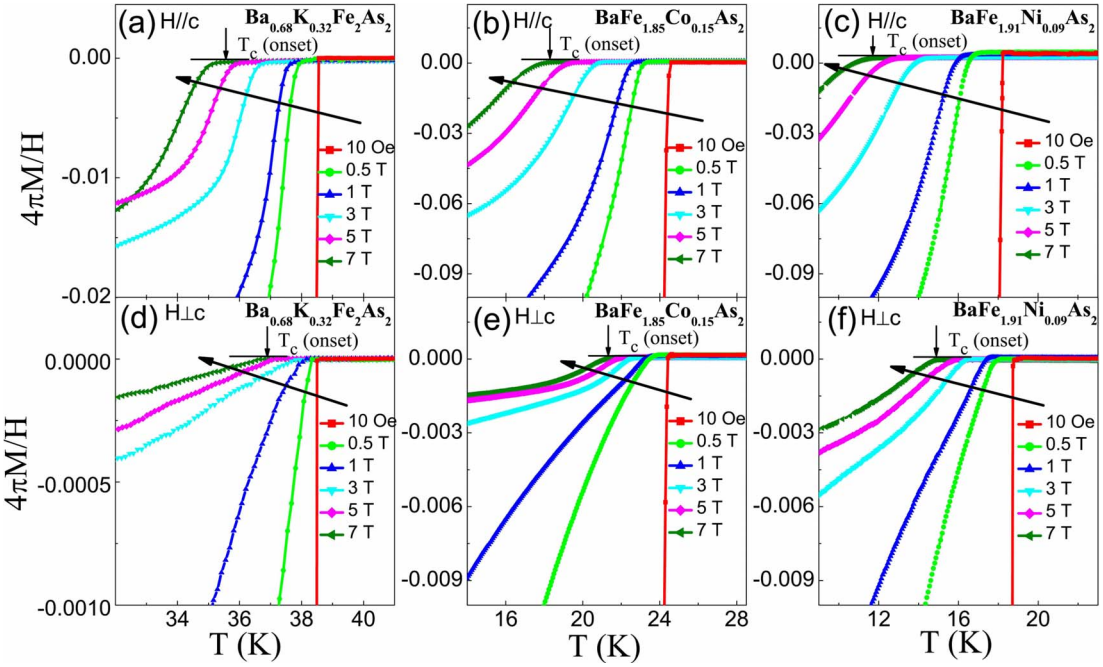

FIG. 2. (Color online) Temperature dependence of the magnetic susceptibility for both $H\|c$ and $H\perp c$ configurations under various magnetic fields. The data were recorded using zero-field-cooling cycles. (a) and (d) for $Ba_{0.68}K_{0.32}Fe_2As_2$, (b) and (e) for $BaFe_{1.85}Co_{0.15}As_2$, and (c) and (f) for $BaFe_{1.91}Ni_{0.09}As_2$ single crystals, respectively.

$BaFe_{1.91}Ni_{0.09}As_2$ crystals. The in-plane coherence length $\xi_{ab}(0)$ and the c-axis coherence length $\xi_c(0)$ are estimated to be 1.92–3.36 and 0.92–1.37 nm, deduced by the Ginzburg–Landau relations, respectively.

The anisotropic ratio of $\gamma = H_{c2}^{\perp c}/H_{c2}^{\|c}$ was determined both resistive and magnetic data, as shown in Figs. 3(d)–3(f), respectively. The value of γ decreases to ~2.5 for $Ba_{0.68}K_{0.32}Fe_2As_2$, ~3.0 for $BaFe_{1.85}Co_{0.15}As_2$ and $BaFe_{1.91}Ni_{0.09}As_2$, respectively. The anisotropic ratio γ obtained by the magnetic-susceptibility measurements are consistent with the resistive ones. These results indicate that either hole-doped (out-of-plane) or electron-doped (in-plane)

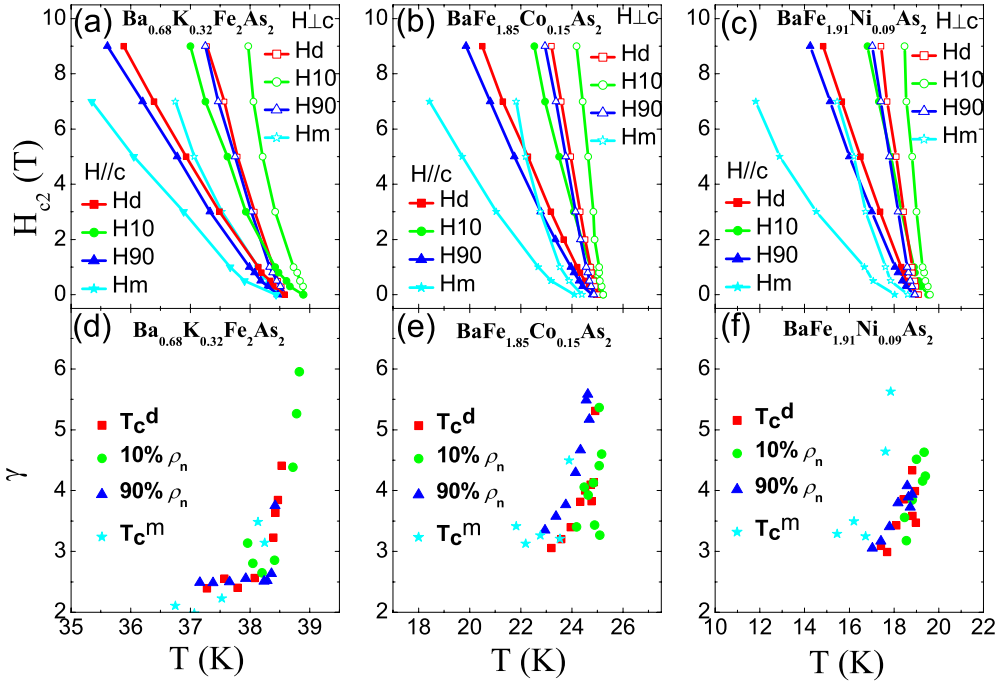

FIG. 3. (Color online) The upper critical field H_{c2} obtained by varying definitions. (a) $Ba_{0.68}K_{0.32}Fe_2As_2$, (b) $BaFe_{1.85}Co_{0.15}As_2$, and (c) $BaFe_{1.91}Ni_{0.09}As_2$ single crystals for both $H\|c$ and $H\perp c$ configurations, respectively. [(d)–(f)] The anisotropic ratio γ of H_{c2} from the two magnetic field orientations for the three single crystals, respectively.

TABLE I. The slope dH_{c2}/dT, zero-temperature upper critical fields $H_{c2}(0)$, coherence lengths ξ, and critical current density J_c for $Ba_{0.68}K_{0.32}Fe_2As_2$, $BaFe_{1.85}Co_{0.15}As_2$, and $BaFe_{1.91}Ni_{0.09}As_2$ single crystals.

	dH_{c2}/dT		$H_{c2}(0)$		ξ (nm)		
Crystals	$H\|c$	$H\perp c$	$H\|c$ (T)	$H\perp c$ (T)	ξ_{ab}	ξ_c	J_c at 10 K, 0 T (10^6 A/cm^2)
$Ba_{0.68}K_{0.32}Fe_2As_2$	−3.37	−6.97	89	185	1.92	0.92	1.07
$BaFe_{1.85}Co_{0.15}As_2$	−2.04	−5.08	35	88	3.05	1.10	0.42
$BaFe_{1.91}Ni_{0.09}As_2$	−2.19	−5.42	29	71	3.36	1.37	0.23

FeAs conductor layer exhibits relative small γ and nearly isotropic property.

The MHLs for the three samples was obtained by$H\|c$ at various temperatures, as shown in Figs. 4(a)–4(c). The second magnetization peak H_{sp}, namely, fishtail effect, can be clearly observed in all three samples, as shown in Figs. 4(a)–4(c), respectively. By fitting the plot of H_{sp} vs T, a power-law behavior in the $Ba_{0.6}K_{0.4}Fe_2As_2$ (Ref. 23) compared with that of $YBa_2Cu_3O_{7-\delta}$ superconductor with oxygen deficiency defects as observed.[24] Thus the fishtail effect was suggested to be originated from the small-size normal-core pinning effect. It should be stressed that second peak disappears in the field of $H\perp c$.[25] This suggests an effect of anisotropic flux pinning. Based on the analysis of the temperature and field dependencies of the magnetic relaxation, the second peak is suggested to be resulted by a crossover from the elastic collective creep to the plastic vortex creep.[25]

The field dependence of critical current density J_c was estimated by the MHLs according to the Bean model[26] $J_c = 20\Delta M/[w(1-w/3l)]$, where ΔM is in the unit of emu/cm^3, l is the length, and w is the width for the sample, respectively. The field dependence of J_c for $Ba_{0.68}K_{0.32}Fe_2As_2$, $BaFe_{1.85}Co_{0.15}As_2$, and $BaFe_{1.91}Ni_{0.09}As_2$ single crystals is shown in Figs. 4(d)–4(f), respectively. The estimated J_c at 10 K is listed in Table I. High critical current density of $\sim 10^5$–10^6 A/cm^2 indicates a promising application for the compounds. The J_c values of hole-doped $Ba_{0.68}K_{0.32}Fe_2As_2$ are about 2–4 times larger than those of electron-doped $BaFe_{1.85}Co_{0.15}As_2$ and $BaFe_{1.91}Ni_{0.09}As_2$ single crystals. Therefore the hole-doped compound displays a promising application in the production of high magnetic fields.

Figures 5(a)–5(c) show the temperature-normalized (T/T_c) vortex phase diagrams. The H_{c2} and H_{sp} shift toward high-temperature and the higher field region for $Ba_{0.68}K_{0.32}Fe_2As_2$, indicating a stronger vortex pinning in the compound. Recently, a highly disordered vortex configuration was observed by small-angle neutron scattering and it was attributed to the strong pinning. The results indicate that

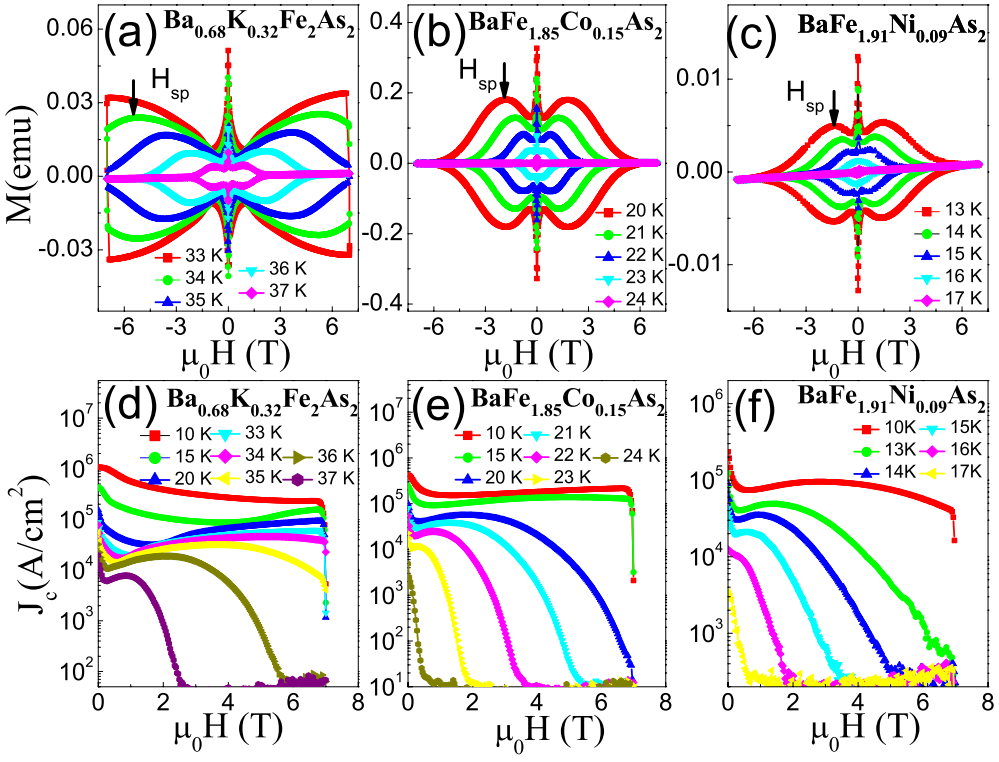

FIG. 4. (Color online) MHLs for (a) $Ba_{0.68}K_{0.32}Fe_2As_2$, (b) $BaFe_{1.85}Co_{0.15}As_2$, and (c) $BaFe_{1.91}Ni_{0.09}As_2$ single crystals at different temperatures. Second magnetization peak H_{sp} appears close to T_c for all three samples. (d), (e), and (f) are the critical current density J_c calculated from the Bean model for the above three crystals.

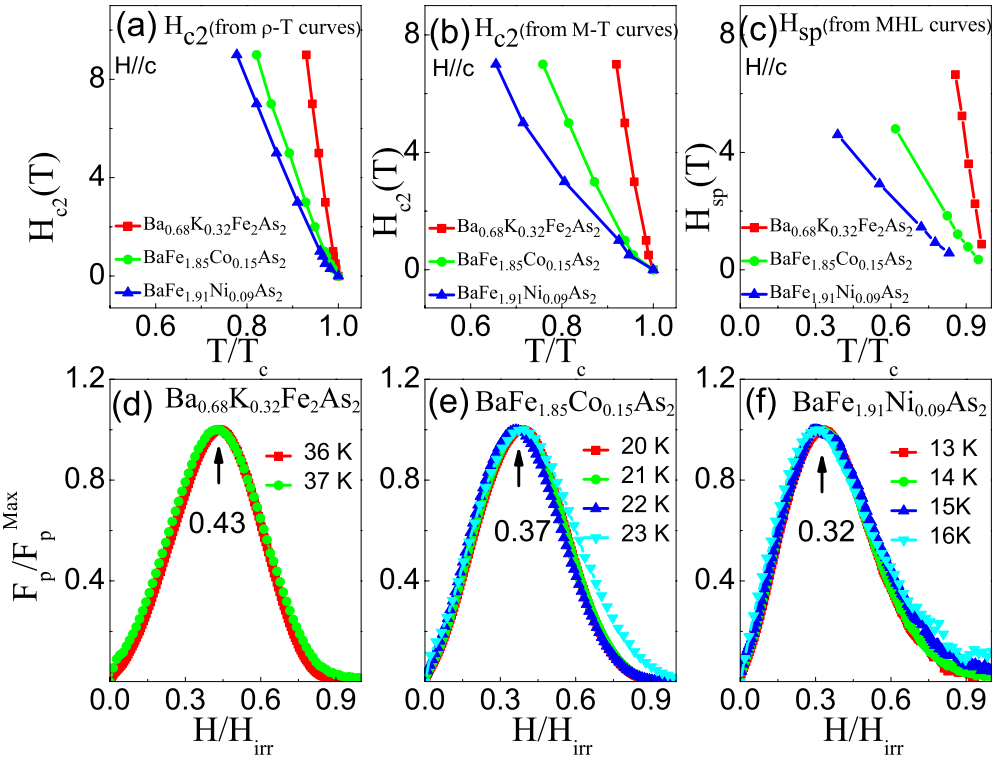

FIG. 5. (Color online) Temperature-normalized (T/T_c) vortex phase diagrams for $Ba_{0.68}K_{0.32}Fe_2As_2$, $BaFe_{1.85}Co_{0.15}As_2$, and $BaFe_{1.91}Ni_{0.09}As_2$ single crystals. (a) H_{c2} obtained from ρ-T curves, (b) H_{c2} obtained from M-T curves, and (c) H_{sp} obtained from MHLs. Scaling behavior of the normalized pinning force F_p/F_p^{Max} vs reduced field $h=H/H_{irr}$ at different temperatures for (d) $Ba_{0.68}K_{0.32}Fe_2As_2$; (e) $BaFe_{1.85}Co_{0.15}As_2$, and(f) $BaFe_{1.91}Ni_{0.09}As_2$ single crystals, respectively.

the iron-based superconductors are the strongly disordered compounds containing randomly orientated vortex lattice domains.[27] In order to compare the strength of vortex pinning we doped in (electron-doped) and out-of (hole-doped) plane of the FeAs. Our results give evidence that the hole-doped sample with higher T_c displays a stronger vortex pinning which seems only related to the stiffness of superconductivity, in spite of doping levels in the sample. The electron-doped compounds provide charge carriers for inducing superconductivity, but they do not introduce additional disorders serving as pinning centers.

To study the pinning mechanisms in iron-based superconductors, the scaling behavior of the pinning forces at different temperatures against the reduced field $h=H/H_{irr}$ was plotted in Figs. 5(d)–5(f), respectively. The pinning force was obtained from the critical current density as $F_p=\mu_0 H J_c$, and F_p^{Max} corresponds to the maximum pinning force. H_{irr} is defined as irreversibility field at which $J_c(H)$ extrapolates to zero. The behavior of the normalized pinning force, F_p/F_p^{Max}, is observed to be well overlapped at the peak positions of $h\sim 0.43$, 0.37, and 0.32 under the reduced magnetic field, $h=H/H_{irr}$ for $Ba_{0.68}K_{0.32}Fe_2As_2$, $BaFe_{1.85}Co_{0.15}As_2$, and $BaFe_{1.91}Ni_{0.09}As_2$ single crystals, respectively.

For the classical type-II superconductors, the universal scaling behavior was used to analyze the types of pinning centers,[28] i.e., the maximum of $h=0.2$ corresponds to the grain-boundaries pinning, $h\sim 0.33$ to the point defects pinning and $h=0.7$ to the pinning by spatial variations in the order parameter.[28] Yang *et al.* suggested that the observed value of $h=0.33$ should be for the small size normal cores in the $Ba_{0.6}K_{0.4}Fe_2As_2$ such as arsenic deficiency,[10] being analogous to the oxygen deficiency defects in the $YBa_2Cu_3O_{7-\delta}$.[24] For the compound of $BaFe_{1.8}Co_{0.2}As_2$ a peak at $h\sim 0.45$ was suggested to be related to the inhomogeneous distribution of Co ions.[16] It is noticed that H_{c2} and H_{sp} decrease faster with decreasing temperature for the Ni-doped $BaFe_{1.91}Ni_{0.09}As_2$ than that for K- and Co-doped samples. Therefore the Ni-doped sample seems to be inhomogenous, which was indicated by the larger ΔT_c compared to the K- and Co-doped samples. Nevertheless, the hole-doped $Ba_{0.68}K_{0.32}Fe_2As_2$ shows the strongest pinning and the quality is proven to be the best among the three kinds of crystals. Therefore, the As deficiency or inhomogeneous distribution of dopant could not play a key role in determining the strong pinning in iron-based superconductors.

It is noticed that the presence of complex domain structures were confirmed in the parent compounds of AFe_2As_2 (A=Sr,Ca) by transmission electron microscopy.[29] Moreover, using a combination of polarized light microscopy and spatially resolved high-energy synchrotron x-ray diffraction, the structural domains due to the orthorhombic distortion were observed directly, which has been suggested to be responsible for the intrinsic disorder and anisotropy of iron arsenides.[30] Recently, Prozorov *et al.*[31] described that the intertwined orthorhombic magnetic/structural domains would give rise to the strong intrinsic pinning in the underdoped regime for the $Ba(Fe_{1-x}Co_x)_2As_2$. For the optimally doped compounds it shows no evidence for existence of the disor-

dered structural domains, but much finer structural domains could play a role to determine the vortex pinning. $Ba_{0.68}K_{0.32}Fe_2As_2$ single crystal displays the strongest pinning because it has the most fluctuating domains. This picture appeals the strongly disordered vortex pattern obtained by STM and neutron-scattering measurements in iron-based superconductors.

IV. CONCLUSIONS

A comparative study of the upper critical field H_{c2} and critical current density J_c has been performed using high-quality single crystals of $Ba_{0.68}K_{0.32}Fe_2As_2$, $BaFe_{1.85}Co_{0.15}As_2$, and $BaFe_{1.91}Ni_{0.09}As_2$. We confirmed that both hole- and electron-doped samples have small γ, high $H_{c2}(0)$, and large J_c. The high $H_{c2}(0)$ and J_c are observed in the hole-doped $Ba_{0.68}K_{0.32}Fe_2As_2$ and estimated to be 2–4 times larger than those of the electron-doped $BaFe_{1.85}Co_{0.15}As_2$ and $BaFe_{1.91}Ni_{0.09}As_2$. We propose that the strong vortex pinning could result from the fluctuating magnetic/structural domains.

ACKNOWLEDGMENT

We thank G. Götz for the XRD measurements, C. Busch for the analysis of crystal composition, and L. Dorner-Finkbeiner and H. Bender for technical support.

[1] N. R. Werthamer, E. Helfand, and P. C. Hohenberg, Phys. Rev. **147**, 295 (1966).
[2] W. E. Lawrence and S. Doniach, *Proceedings of the 12th International Conference on Low Temperature Physics*, Kyoto, 1970, edited by E. Kanda (Keigaku, Tokyo, 1971), p. 361.
[3] Y. Kamihara, T. Watanabe, M. Hirano, and H. Hosono, J. Am. Chem. Soc. **130**, 3296 (2008).
[4] F. Hunte, J. Jaroszynski, A. Gurevich, D. C. Larbalestier, R. Jin, A. S. Sefat, M. A. McGuire, B. C. Sales, D. K. Christen, and D. Mandrus, Nature (London) **453**, 903 (2008).
[5] Y. Jia, P. Cheng, L. Fang, H. Luo, H. Yang, C. Ren, L. Shan, C. Gu, and H.-H. Wen, Appl. Phys. Lett. **93**, 032503 (2008).
[6] U. Welp, R. Xie, A. E. Koshelev, W. K. Kwok, P. Cheng, L. Fang, and H.-H. Wen, Phys. Rev. B **78**, 140510(R) (2008).
[7] J. Jaroszynski, F. Hunte, L. Balicas, Youn-jung Jo, I. Raicevic, A. Gurevich, D. C. Larbalestier, F. F. Balakirev, L. Fang, P. Cheng, Y. Jia, and H.-H. Wen, Phys. Rev. B **78**, 174523 (2008).
[8] N. Ni, S. L. Bud'ko, A. Kreyssig, S. Nandi, G. E. Rustan, A. I. Goldman, S. Gupta, J. D. Corbett, A. Kracher, and P. C. Canfield, Phys. Rev. B **78**, 014507 (2008).
[9] Z.-S. Wang, H.-Q. Luo, C. Ren, and H.-H. Wen, Phys. Rev. B **78**, 140501(R) (2008).
[10] H.-J. Kim, Y. Liu, Y. S. Oh, S. H. Khim, I. Kim, G. R. Stewart, and K. H. Kim, Phys. Rev. B **79**, 014514 (2009).
[11] M. M. Altarawneh, K. Collar, C. H. Mielke, N. Ni, S. L. Bud'ko, and P. C. Canfield, Phys. Rev. B **78**, 220505(R) (2008).
[12] U. Welp, R. Xie, A. E. Koshelev, W. K. Kwok, H. Q. Luo, Z. S. Wang, G. Mu, and H.-H. Wen, Phys. Rev. B **79**, 094505 (2009).
[13] H. Q. Yuan, J. Singleton, F. F. Balakirev, S. A. Baily, G. F. Chen, J. L. Luo, and N. L. Wang, Nature (London) **457**, 565 (2009).
[14] N. Ni, M. E. Tillman, J.-Q. Yan, A. Kracher, S. T. Hannahs, S. L. Bud'ko, and P. C. Canfield, Phys. Rev. B **78**, 214515 (2008).
[15] M. A. Tanatar, N. Ni, C. Martin, R. T. Gordon, H. Kim, V. G. Kogan, G. D. Samolyuk, S. L. Bud'ko, P. C. Canfield, and R. Prozorov, Phys. Rev. B **79**, 094507 (2009).
[16] A. Yamamoto, J. Jaroszynski, C. Tarantini, L. Balicas, J. Jiang, A. Gurevich, D. C. Larbalestier, R. Jin, A. S. Sefat, M. A. McGuire, B. C. Sales, D. K. Christen, and D. Mandrus, Appl. Phys. Lett. **94**, 062511 (2009).
[17] G. L. Sun, D. L. Sun, M. Konuma, P. Popovich, A. Boris, J. B. Peng, K. Y. Choi, P. Lemmens, and C. T. Lin, arXiv:0901.2728 (unpublished).
[18] D. L. Sun, Y. Liu, J. T. Park, and C. T. Lin, Supercond. Sci. Technol. **22**, 105006 (2009).
[19] M. Rotter, M. Pangerl, M. Tegel, and D. Johrendt, Angew. Chem., Int. Ed. **47**, 7949 (2008).
[20] H. Chen, Y. Ren, Y. Qiu, W. Bao, R. H. Liu, G. Wu, T. Wu, Y. L. Xie, X. F. Wang, Q. Huang, and X. H. Chen, EPL **85**, 17006 (2009).
[21] J. H. Chu, J. G. Analytis, C. Kucharczyk, and I. R. Fisher, Phys. Rev. B **79**, 014506 (2009).
[22] L. J. Li, Y. K. Luo, Q. B. Wang, H. Chen, Z. Ren, Q. Tao, Y. K. Li, X. Lin, M. He, Z. W. Zhu, G. H. Cao, and Z. A. Xu, New J. Phys. **11**, 025008 (2009).
[23] H. Yang, H. Luo, Z. Wang, and H.-H. Wen, Appl. Phys. Lett. **93**, 142506 (2008).
[24] L. Klein, E. R. Yacoby, Y. Yeshurun, A. Erb, G. Müller-Vogt, V. Breit, and H. Wühl, Phys. Rev. B **49**, 4403(R) (1994).
[25] R. Prozorov, N. Ni, M. A. Tanatar, V. G. Kogan, R. T. Gordon, C. Martin, E. C. Blomberg, P. Prommapan, J. Q. Yan, S. L. Bud'ko, and P. C. Canfield, Phys. Rev. B **78**, 224506 (2008).
[26] C. P. Bean, Rev. Mod. Phys. **36**, 31 (1964).
[27] M. R. Eskildsen, L. Ya. Vinnikov, T. D. Blasius, I. S. Veshchunov, T. M. Artemova, J. M. Densmore, C. D. Dewhurst, N. Ni, A. Kreyssig, S. L. Bud'ko, P. C. Canfield, and A. I. Goldman, Phys. Rev. B **79**, 100501(R) (2009).
[28] D. Dew-Hughes, Philos. Mag. **30**, 293 (1974).
[29] C. Ma, H. X. Yang, H. F. Tian, H. L Shi, J. B. Lu, Z. W. Wang, L. J. Zeng, G. F. Chen, N. L. Wang, and J. Q. Li, Phys. Rev. B **79**, 060506(R) (2009).
[30] M. A. Tanatar, A. Kreyssig, S. Nandi, N. Ni, S. L. Bud'ko, P. C. Canfield, A. I. Goldman, and R. Prozorov, Phys. Rev. B **79**, 180508(R) (2009).
[31] R. Prozorov, M. A. Tanatar, N. Ni, A. Kreyssig, S. Nandi, S. L. Bud'ko, A. I. Goldman, and P. C. Canfield, arXiv:0909.0923 (unpublished).